

Enhancing Carbon Emission Reduction Strategies using OCO and ICOS data

Oskar Åström

Alexandros Sopasakis

Centre for Mathematical Sciences

Lund University

221 00 Lund, Sweden

Carina Geldhauser

Munich Center for Machine Learning

Technical University of Munich

85748 Garching, Germany

Markus Grillitsch

Ola Hall

Department of Human Geography

Lund University

221 00 Lund, Sweden

OSKAR.ASTROM@MATH.LTH.SE

ALEXANDROS.SOPASAKIS@MATH.LTH.SE

CARINA.GELDHAUSER@MA.TUM.DE

MARKUS.GRILLITSCH@KEG.LU.SE

OLA.HALL@KEG.LU.SE

Editor: TBD

Abstract

We propose a methodology to enhance local CO₂ monitoring by integrating satellite data from the Orbiting Carbon Observatories (OCO-2 and OCO-3) with ground level observations from the Integrated Carbon Observation System (ICOS) and weather data from the ECMWF Reanalysis v5 (ERA5). Unlike traditional methods that downsample national data, our approach uses multimodal data fusion for high-resolution CO₂ estimations.

We employ weighted K-nearest neighbor (KNN) interpolation with machine learning models to predict ground level CO₂ from satellite measurements, achieving a Root Mean Squared Error of 3.92 ppm. Our results show the effectiveness of integrating diverse data sources in capturing local emission patterns, highlighting the value of high-resolution atmospheric transport models. The developed model improves the granularity of CO₂ monitoring, providing precise insights for targeted carbon mitigation strategies, and represents a novel application of neural networks and KNN in environmental monitoring, adaptable to various regions and temporal scales.

Keywords: Carbon Emission Monitoring, ICOS, Machine Learning, OCO-2 and OCO-3, Remote Sensing, Ground Level CO₂

1 Introduction

In this era of rapid climate change, the precise monitoring of carbon dioxide emissions has become a critical task for governing bodies and environmental organizations worldwide. The ability to accurately assess and manage CO₂ levels is not just a scientific challenge, but a necessity for effective climate action.

The current landscape of carbon dioxide (CO₂) measurement is fraught with challenges, predominantly due to the lack of comprehensive and localized data. Local authorities, which are on the front line of implementing climate action strategies, often find themselves relying on national-level data or extrapolations from limited ground measurements. This lack of granularity in the data can lead to inaccuracies in identifying local emission sources, while also impeding the development of more effective, targeted, climate strategies.

Our research aims to bridge this gap by using satellite-derived data to provide a more precise and localized view of CO₂ emissions. We adopt a multimodal data approach, utilizing data from the Orbiting Carbon Observatories (OCO-2 and OCO-3) as well as the Integrated Carbon Observation System (ICOS) and the ECMWF Reanalysis v5 (ERA5) model, enabling us to establish vital connections between satellite transects, ground level CO₂ data, and weather. This integration is pivotal in enhancing the precision and reliability of CO₂ datasets derived from satellite observations, offering an unprecedented level of detail in emission monitoring.

In technical terms, our aim is to build a machine learning algorithm which, using satellite data for carbon dioxide, weather, and other relevant input factors, can model accurate measurements, similar to ICOS ground data measurements of the biospheric surface CO₂ flux anomalies.

However, monitoring of CO₂ using satellite data is not without its challenges. Unlike pollutants with relatively short atmospheric lifetimes such as NO₂ and SO₂, CO₂ has a longer lifespan, resulting in a high background concentration that complicates the identification of new anthropogenic sources. Furthermore, the spatiotemporal distribution of CO₂ is heavily influenced by atmospheric dynamics and terrestrial biospheric fluxes, introducing significant variability and seasonality in measurements.

Although significant strides have been made in atmospheric CO₂ monitoring, the complexity of the task remains, with challenges in regions of complex topography and varying meteorological conditions. Continuous advancements in satellite technology, data processing, and atmospheric modeling are crucial to enhance the accuracy and scope of global CO₂ monitoring.

Our methodology addresses these challenges by creating machine learning models that employ advanced statistical analyses to estimate ground observations of CO₂ from satellite data. We also explore the utility of high-resolution satellite data in capturing small-scale variability of CO₂, which is often lost in coarser-resolution models. This approach is critical in understanding the nuances of CO₂ weather - the interaction between weather patterns and CO₂ surface fluxes – and in providing accurate data for regional modeling studies and field experiments. We begin in Section 2 with an overview of satellite-based CO₂ monitoring approaches and their utilization in CO₂ estimation.

Then, in Section 2.2 we describe current methodological advances as well as challenges in the data collected from the OCO-2 and OCO-3 satellites. We then describe in more

detail the methods and data used in this work in Section 3. We present our findings and end with a feature importance analysis of the models in Section 4.

2 State of the art

In this section, we provide an overview of key satellite instruments that have significantly advanced the field of CO₂ monitoring. We discuss the specific contributions of satellites such as SCIAMACHY, GOSAT, and OCO-2, highlighting their roles in improving the precision of CO₂ measurements and their applications in environmental research. The discussion includes an analysis of how these satellites have been utilized to detect CO₂ emissions from various sources, understand the effects of atmospheric transport on CO₂ distribution, and enhance our overall understanding of the global carbon cycle.

In recent decades, significant advances have been made in satellite technology for environmental monitoring. Notable among these are instruments like SCIAMACHY (Scanning Imaging Absorption Spectrometer for Atmospheric Chartography) onboard the Environmental Satellite, ENVISAT, operational from 2002 to 2012 and the Greenhouse Gases Observing Satellite (GOSAT), launched in 2009. These satellites, along with others such as the American OCO-2, the Chinese TanSat, and the upcoming Geostationary Carbon Observatory (GeoCarb), have revolutionized our ability to monitor atmospheric CO₂. Each of these satellites offers unique contributions to the field, from high-precision CO₂ observing capabilities to the monitoring of CO₂ variations on seasonal time scales.

The analysis of data collected by SCIAMACHY has been instrumental in deriving empirical regional conversion factors, which are used to estimate CO₂ emissions based on observed NO₂ columns. This approach, as demonstrated in previous studies Schneising et al. (2014); Reuter et al. (2014), helps establish a crucial link between NO₂—a short-lived pollutant indicative of fossil fuel combustion—and the longer-lived CO₂, thereby enhancing our understanding of anthropogenic emissions and their impact on atmospheric composition.

SCIAMACHY data was used also to estimate CO₂ abundance from fossil fuel emissions, particularly from power plants Bovensmann et al. (2010). This approach has provided insights into the spatial distribution of CO₂ emissions, contributing to a more nuanced understanding of anthropogenic impacts on atmospheric CO₂ levels.

Greenhouse gases observing satellite (GOSAT) observations have been pivotal in detecting CO₂ emission signatures from urban centers like Los Angeles and Mumbai Kort et al. (2012); Yokota et al. (2009). This detection capability is crucial for understanding the role of megacities in global CO₂ emissions. These satellite-based CO₂ abundances can be compared with emission inventories, revealing potential gaps in emission estimates, as was shown in a study from East Asia Janardanan et al. (2016).

The capabilities of OCO-2 surpass those of earlier instruments such as SCIAMACHY and GOSAT, particularly due to a significant reduction in xCO₂ retrieval uncertainty. This reduction is achieved through OCO-2’s higher spectral resolution, advanced data processing algorithms, and improved spatial and temporal coverage. As a result, OCO-2 provides more precise and reliable measurements of CO₂, enhancing our ability to monitor global emissions, validate emission inventories, and improve climate models, thereby deepening our understanding of CO₂’s role in climate change.

Feldman et al. (2023) showed that OCO-2 can also detect anomalies arising from terrestrial biosphere extremes, for example droughts and heat waves with a rate of 80% in some parts of Northern Australia and 'greater than by chance' detection rates for the most extreme CO₂ surface flux anomalies in western US (Feldman et al. (2023), page 1555). This advancement is crucial for detecting subtle CO₂ anomalies that may be indicative of significant environmental events or trends.

2.1 Challenges in CO₂ emissions estimation

Carbon dioxide presents unique challenges due to its longer atmospheric lifespan and high background concentration, which complicates the identification of anthropogenic sources (Hakkarainen et al. (2023); Bovensmann et al. (2010); Keppel-Aleks et al. (2013)). The bottom-up compilation of CO₂ inventories, based on reported data or human activity such as energy consumption and fuel purity, faces notable discrepancies in emission estimates. These uncertainties are especially pronounced in megacities in developing countries (Peylin et al. (2013); Wang et al. (2013)).

Due to its longer lifespan, atmospheric transport of CO₂ becomes a relevant factor, which can lead to overestimation in deserts and underestimation in areas with significant vegetation, as indicated by He et al. (2018). Their study highlights how extreme changes in atmospheric CO₂ concentrations, detected using satellite data, are influenced by local environmental conditions and transport dynamics, underscoring the complexity of accurately estimating CO₂ levels in diverse regions.

The variability of atmospheric CO₂ is heavily influenced by its interaction with weather patterns, which requires high-resolution atmospheric transport models. These models are critical for capturing small-scale variability and understanding the intricacies of CO₂ weather (Feldman et al. (2023)). However, monitoring global carbon sources and sinks is highly complex and needs to quantify longer latency and errors due to assumptions about uncertain surface CO₂ flux drivers and meteorological conditions (Feldman et al. (2023)).

The integration of weather data, as explored by Hakkarainen et al. (2023), Beirle et al. (2011), and Fioletov et al. (2015), offers a more comprehensive understanding of emissions, particularly from isolated urban areas. Incorporating wind speed information is crucial for interpreting emission patterns and understanding the dynamics of pollutant dispersion. Research indicates the need for undisturbed atmospheric transport for accurate xCO₂ retrievals, highlighting the need for low variability in wind direction and speed, a consistent wind source and the avoidance of complex topography near the surface (Hakkarainen et al. (2023); Beirle et al. (2011); Fioletov et al. (2015); Feldman et al. (2023)).

2.2 OCO-2 and OCO-3: Advances and Challenges in CO₂ Monitoring

The Orbiting Carbon Observatory satellites, OCO-2 and OCO-3, represent a significant advancement in the global monitoring of carbon dioxide (CO₂). Unlike direct measurement techniques, these satellites detect CO₂ by measuring the absorption of sunlight reflected from the Earth's surface within an air column (Eldering et al. (2017); Taylor et al. (2023)). This approach, combined with their high sensitivity, enables these satellites to provide detailed insights into atmospheric CO₂ concentrations. The measurement area for OCO-2

and OCO-3 is approximately 1.29×2.25 km, achieved through a sun-synchronous orbit that ensures consistent data acquisition across different regions Feldman et al. (2023).

A key strength of OCO-2 and OCO-3 lies in their ability to generate column-averaged dry-air mole fractions of CO_2 . This is accomplished through advanced retrieval algorithms, which integrate point measurements to produce highly accurate data for further analysis OCO (2023). The precision of these satellites has been instrumental in urban emission monitoring, particularly in evaluating fossil fuel CO_2 emissions from densely populated areas. High-resolution transport modeling, combined with Bayesian inversion systems, has been used to optimize city-wide emission estimates Ye et al. (2020). Furthermore, the Snapshot Area Mapping (SAM) mode of OCO-3 has proven effective in characterizing major anthropogenic sources, especially when supplemented with NO_2 measurements from other satellite instruments Hakkarainen et al. (2023).

However, despite these advancements, OCO-2 and OCO-3 face several challenges that limit their effectiveness in certain scenarios. Firstly, their sun-synchronous orbits and narrow measurement swaths restrict the frequency and coverage of observations over specific regions, especially concerning point sources such as power plants, where emission origins are concentrated to a single location.

Additionally, both satellites are subject to retrieval errors and observation gaps, which can hinder the consistent detection of flux anomalies, particularly in complex terrains or under specific atmospheric conditions Taylor et al. (2023). The accuracy of data can also be affected by biases introduced through small pointing errors, especially in regions with rough topography. Therefore, rigorous data filtering and bias correction, calibrated against standards like TCCON and the WMO CO_2 reference scale, are crucial to maintaining data integrity OCO (2023).

The modeling of point sources, such as coal power plants Feldman et al. (2023), further highlights the challenges associated with satellite-based CO_2 monitoring. For instance, several studies O’Dell et al. (2018); Claeyman et al. (2011); Wang et al. (2022) have shown that a significant proportion of satellite data can be rendered unusable due to unfavorable atmospheric conditions, such as cloud cover, aerosols, or haze, which obscure the satellite’s view and lead to retrieval errors. Even when data retrieval is successful, such measurements may fail to capture information near or even downwind of the emission source due to, for instance, sudden changes in wind speed and misalignment between the emission source and the detected plume Feldman et al. (2023). These factors underscore the need for continuous refinement of satellite-based CO_2 monitoring techniques in order to improve data reliability and accuracy.

While OCO-2 and OCO-3 have significantly advanced our capability to monitor global CO_2 emissions, ongoing challenges in data retrieval, particularly over complex terrains and smaller emission sources, underscore the need for continued refinement in both satellite technology and data processing methodologies.

3 Materials and Methods

This study uses data from multiple openly available high-resolution datasets, providing comprehensive measurements of the CO_2 concentration and the atmospheric variable, which we describe in the following section.

3.1 Datasets

We began by employing OCO-2 and OCO-3 satellite data consisting of bias-corrected, retrospective $x\text{CO}_2$ measurements from the Level 2 mission¹. To ensure accuracy and reliability, this data is pre-processed at the source by the OCO-2 and OCO-3 Science Teams at NASA and associated institutions Team et al. (2020). This pre-processing also includes physics-based algorithms to adjust for systematic errors through bias correction and produce improved measurements of the mole fraction of CO_2 in dry air, as determined from the sun absorption spectra in the near-infrared at 1.61 and 2.06 μm . The satellite data, characterized by a spatial resolution within a one-hour time frame, covers a parallelogram-shaped area of 2.29 km^2 per column with an orbit track width of 10.3 km. Due to the slow nature of API requests, the retrieval of weather data was performed on a one-degree latitude and longitude grid and restricted to a six-hour window from 9:00 to 15:00.

Second, we utilized ICOS station data, incorporating measurements from 32 ICOS atmospheric stations across Europe since 2017. These stations provide hourly averages of dry-air mole fractions of CO_2 . They employ nondispersive infrared (NDIR) analyzers for the spectral analysis of air samples. Unlike the OCO dataset, ICOS data are geographically fixed and offer continuous time series data. However, it is important to note that the recordings are not always complete due to various factors such as instrument malfunctions, power failures, extreme weather conditions, and regular maintenance, which result in interrupted data at most stations.

Third, we used ERA5 Reanalysis Weather Data, sourced from the Copernicus programme and the ECMWF’s Climate Data Store. This dataset provided supplemental weather data, including wind components at 10m height, surface-level pressure, and temperature at 2m. Additional variables such as the vertical integral of temperature and total column water vapor, cloud-based height, and total cloud cover were also included.

The study period spanned from the beginning of the OCO mission in September 2014 to March 2023. The spatial coverage for the weather data for OCO, ICOS and ERA5 was defined within a geodesic rectangle bounded by coordinates 28°S , -17°W , 70°N and 64°E . The sun-synchronous orbit of the OCO satellite resulted in more frequent data collection over European ICOS stations during summer and reduced coverage in winter.

To construct the dataset, satellite measurements from OCO was matched with the closest measurement from a station, if it was within a certain distance in space and time. While the ICOS stations measured continuously, data could only be combined when the satellite passed over which reduced the amount of data drastically. Figure 1 shows the ICOS and OCO measurements for a region around the Hyltemossa ICOS station. The figure shows the small amount of times where there is a corresponding OCO measurement near the station. Figure 1 also shows that the OCO measurements are highly correlated with the ICOS data, as it seems to follow a similar one-year cycle in the CO_2 levels.

To increase the variance in the input data, the OCO measurements were augmented with ERA5 weather data and the location and time information of the measurement. ICOS stations record weather in addition to CO_2 . However, since these stations are geographically fixed and primarily record wind speed and direction, using ICOS data as input prohibits the use of this model outside of the station bounds. Consequently, ERA5 data was used

1. Available at https://disc.gsfc.nasa.gov/datasets/OCO2_L2_Lite_FP_10r/summary

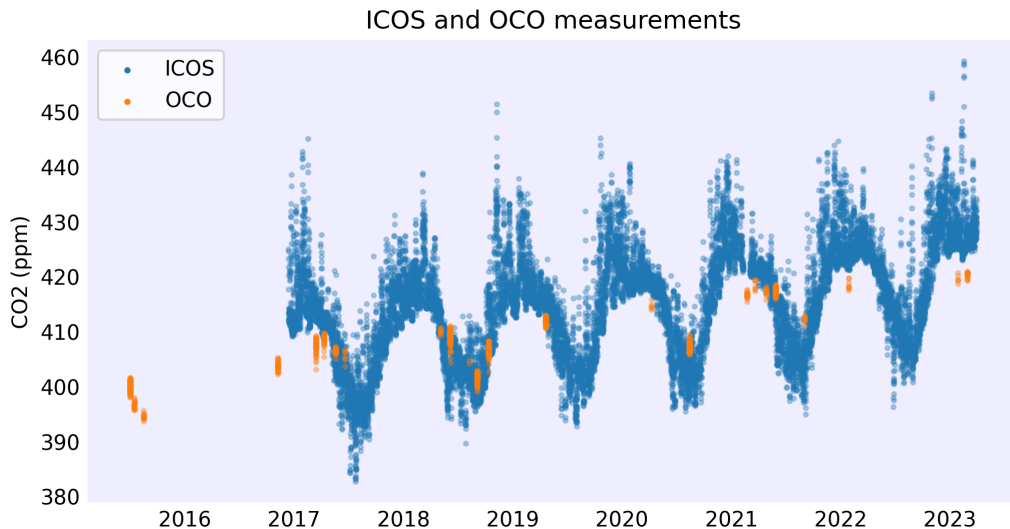


Figure 1: Measurements from the Hyltemossa ICOS station (blue) and nearby OCO observations (orange) within a 25km radius for the time frame of data availability.

for a more comprehensive weather analysis as it has global reach and records more weather features.

3.2 Machine Learning Models

To estimate CO_2 levels from satellite data, we used multiple classes of machine learning models.

As a baseline, we perform simple linear regression on ICOS measurements based only on OCO observations. This baseline therefore does not contain any weather data and is a measurement of how well the OCO satellite data itself correlates with the ground level CO_2 .

Secondly, we employ Boosting models, chosen due to their proven efficacy in handling complex non-linear data relationships, which is characteristic of environmental datasets Wen et al. (2021); Cai et al. (2020). Boosting models in general are a type of ensemble machine learning method designed to improve the accuracy of predictions by combining the outputs of multiple weak learners into a single strong model. The key idea behind boosting is to sequentially train weak models, where each model focuses on correcting the errors made by the previous models in the sequence. The ensemble of weak models therefore is improved by iteratively adding new models that are trained to predict the pseudo-residuals of the previous iteration of the ensemble. These models have been shown to outperform classical methods like Stochastic Gradient Descent and Support Vector Machines in environmental monitoring Cai et al. (2020).

We employed two different types of boosting models; Category Boosting and Extreme Gradient Boosting. Extreme Gradient Boosting is a boosting model that uses continuous input features to describe the data, whereas Category Boosting employs categorical features

and outputs. This discretizes the data into less descriptive but more complex classes, rather than a point in N-dimensional space. The parameters and packages used for Category and Extreme Gradient Boosting are specified in the Appendix.

In addition to employing Boosting models, we utilized a multilayer perceptron (MLP) neural network tailored for regression tasks. This MLP comprises four densely connected hidden layers, encompassing a total of 19,649 trainable parameters—a relatively modest architecture by contemporary standards. This compact model was deliberately chosen due to the nature of the dataset, which includes only 14 features that exhibit strong correlations with the ground truth. Furthermore, since the measurements were exclusively obtained from locations surrounding the ICOS stations, a more complex model would likely lead to significant overfitting to the training data. Further details on the model’s architecture and implementation can be found in the Appendix.

Each model was trained on an identical training set comprising 31,039 data points and evaluated on a test set of 7,584 data points. The test data was sourced from four ICOS stations that were intentionally excluded during training. This strategy was chosen to prevent data leakage — a common pitfall studies that can significantly compromise the validity of the results.

4 Results

In this section, we present the outcomes of our machine learning models applied to satellite and ground-based data for estimating ground level CO₂ concentrations. We first compare the performance of different models, including Category Boosting, Extreme Gradient Boosting, and neural networks, in terms of their accuracy and robustness. This is followed by an analysis of multi-scale CO₂ predictions, extending beyond the ICOS station data to larger geographic areas. Finally, we evaluate the significance of various input features using SHAP analysis, providing insights into the key drivers of the model’s predictions.

4.1 Ground Level CO₂ Estimation

To perform the ground level CO₂ estimation, we used the baseline model, Category Boosting, Extreme Gradient Boosting, and neural network regression as described in Section 3.2.

The baseline model achieved an Root Mean Squared Error (RMSE) of 6.22. This is a measure of the amount of error in the predictions and a low RMSE is desirable. The Category Boosting model exhibited an RMSE of 5.14, while the Extreme Gradient Boosting model, achieved an RMSE of 4.29. Finally, the neural network achieved an RMSE of only 3.92. Table 1 present a comprehensive comparison of these models, including the additional statistical metrics of Mean Squared Error (MSE) and Adjusted R², providing a holistic view of model performances. These results suggest that the neural network is able to capture

more of the variability in the data. These metrics are calculated using

$$\begin{aligned} \text{MSE} &= \frac{1}{n} \sum_{i=1}^n (y_i - \hat{y}_i)^2, \quad \text{RMSE} = \sqrt{\text{MSE}}, \\ R_{\text{adj}}^2 &= 1 - \frac{n-1}{n-p-1} \cdot \frac{\sum_{i=1}^n (y_i - \hat{y}_i)^2}{\sum_{i=1}^n (y_i - \bar{y})^2}, \end{aligned} \quad (1)$$

where n is the number of data points, p is the number of input features, y_i is the true ICOS-measurement, \hat{y}_i is the estimation, and \bar{y} is the average ICOS-measurement.

Table 1: Model comparisons based on metrics in (1).

Model	RMSE	MSE	adj.R2
<i>Baseline</i>	6.22	38.7	0.516
<i>Category Boosting</i>	5.14	26.4	0.671
<i>Gradient Boosting</i>	4.29	18.4	0.769
<i>Neural Regression</i>	3.92	15.3	0.808

To tangibly compare the performance of the neural regression network to the baseline, Figure 2 displays the prediction errors from the two respective models. From the results it is clear that some patterns seen in the baseline are also visible in the neural network predictions. Mainly, Figure 2 shows clear flat sections where prediction errors remain semi-constant in both models. These are satellite measurements that are close in space and time and it is therefore natural that they result in similar predictions. However, it is also clear that the model is effectively able to shift the error of these sections closer to 0 using the additional contextual weather and location data provided.

In addition, Figure 3 illustrates the predictions on the test set. We can infer from this figure that the neural network predictions are somewhat better aligned with the true ICOS measurements, as indicated by their proximity to the diagonal line as well as the lower RMSE score of Table 1. Moreover, the effects of the discretization in the Category Boosting model are apparent in the figure, where the predictions are constrained to a set of fixed values. This is a consequence of the architecture of the Category Boosting methods, which, instead of predicting a value for the ground level CO₂, classifies the measurement as belonging to one of fixed set of possible values. This lowers the resolution of the predictions, but can sometimes be more effective at predictions. This was evidently not the true in this case.

4.2 Multi-scale Predictions

The results above are based on ground truth measurements from ICOS stations, which have a limited geographical reach. However, since the predictive features rely solely on satellite information from ERA5 and OCO satellites, predictions do not need to be confined to just ICOS locations. To do this for a given region and timescale, OCO measurements were collected and combined with the corresponding weather information. These data points were used to make estimates of ground level CO₂ at each point. Since OCO doesn't have

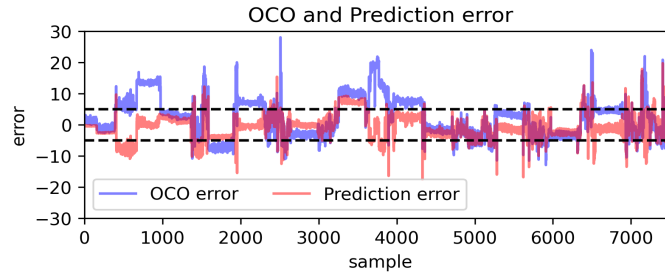


Figure 2: In blue, difference between the actual ICOS and actual OCO measurements. In red, difference between actual ICOS and predicted ICOS. Predictions are produced by the neural network regression model. The dashed lines highlight that most of the predicted values lie within an error of ± 5 ppm.

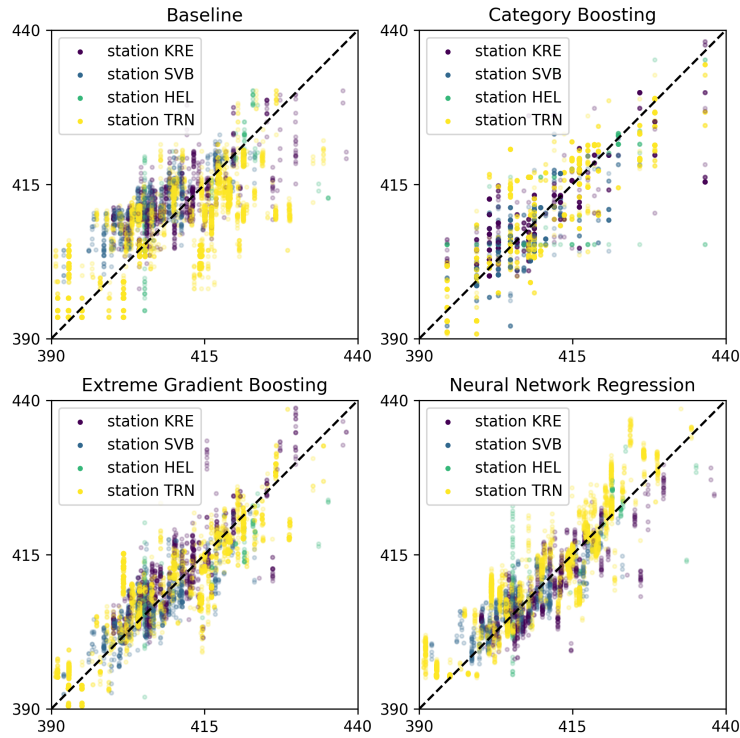


Figure 3: Correspondence plot between the predicted and true CO_2 levels for the test dataset. The x-axis shows the predicted CO_2 level from each respective model, while the y-axis shows to the true ICOS measurement. The locations for each station's acronym listed in the legend can be found at <https://www.icos-cp.eu/observations/station-network>.

full coverage every year, the available measurements have to be interpolated to neighboring locations.

We decided to interpolate the CO₂ levels via a weighted *K-nearest neighbor* (KNN) interpolation method, where the weight function was chosen to be $w = 1/d^p$, where d is the distance to the measurement and p is parameter corresponding to the decay in the weight function. This methodology estimates the value of CO₂ at a given location by considering the values at the K nearest measured locations and assigning weights to them based on their distance from the point of interest.

Specifically, given a set of measurements $\{(x_i, y_i)\}_{i=1}^N$, where x_i represents the location and y_i is the measured CO₂ level at that location, the goal is to estimate the value y^* at a new location x^* . The pseudocode of the proposed methodology is provided in Algorithm 1.

Algorithm 1 Interpolation Procedure

- 1: Identify the K nearest neighbors $\{(x_{i_k}, y_{i_k})\}_{k=1}^K$ to the point x^* based on distance $d(x^*, x_{i_k})$ along the surface of the earth between the point x^* and the k -th neighbor point x_{i_k} .
- 2: Compute the weight w_k for each neighbor based on the distance from x^* , using the weight function

$$w_k = \frac{1}{d(x^*, x_{i_k})^p}, \quad (2)$$

where p is a parameter controlling the decay of the weight with distance.

- 3: Normalize the weights to ensure they sum to 1: $\tilde{w}_k = \frac{w_k}{\sum_{j=1}^K w_j}$, where \tilde{w}_k is the normalized weight for the k -th neighbor.
- 4: The interpolated value y^* at the location x^* is then computed as a weighted sum of the values at the nearest neighbors:

$$y^* = \sum_{k=1}^K \tilde{w}_k y_{i_k}, \quad (3)$$

where y_{i_k} is the measured CO₂ level at the k -th nearest neighbor.

This methodology allows for a more flexible interpolation that adapts to the density and distribution of the measured data, with the parameters K and p providing control over the smoothness and locality of the interpolation. The effect of these parameters can best be understood in the ablation study presented in Figure 4. It was observed that the average CO₂ levels remained relatively constant and close to the mean of the measurements, regardless of the interpolation parameters. However, the standard deviation varied significantly between parameterizations, decreasing as the values of both K and p in (3) and (2) respectively, increased.

The parameter K functions as a smoothing parameter, with a too low K resulting in noise and artifacts from the satellite's orbit, and a too high K removing a lot of the details in the predictions. The parameter p has a small effect when K is also low since measurements are fairly close and thus have a similar distance. However, as K increases, the parameter p has a large effect on the shape of the predictions. We found that using $K = 200$ and

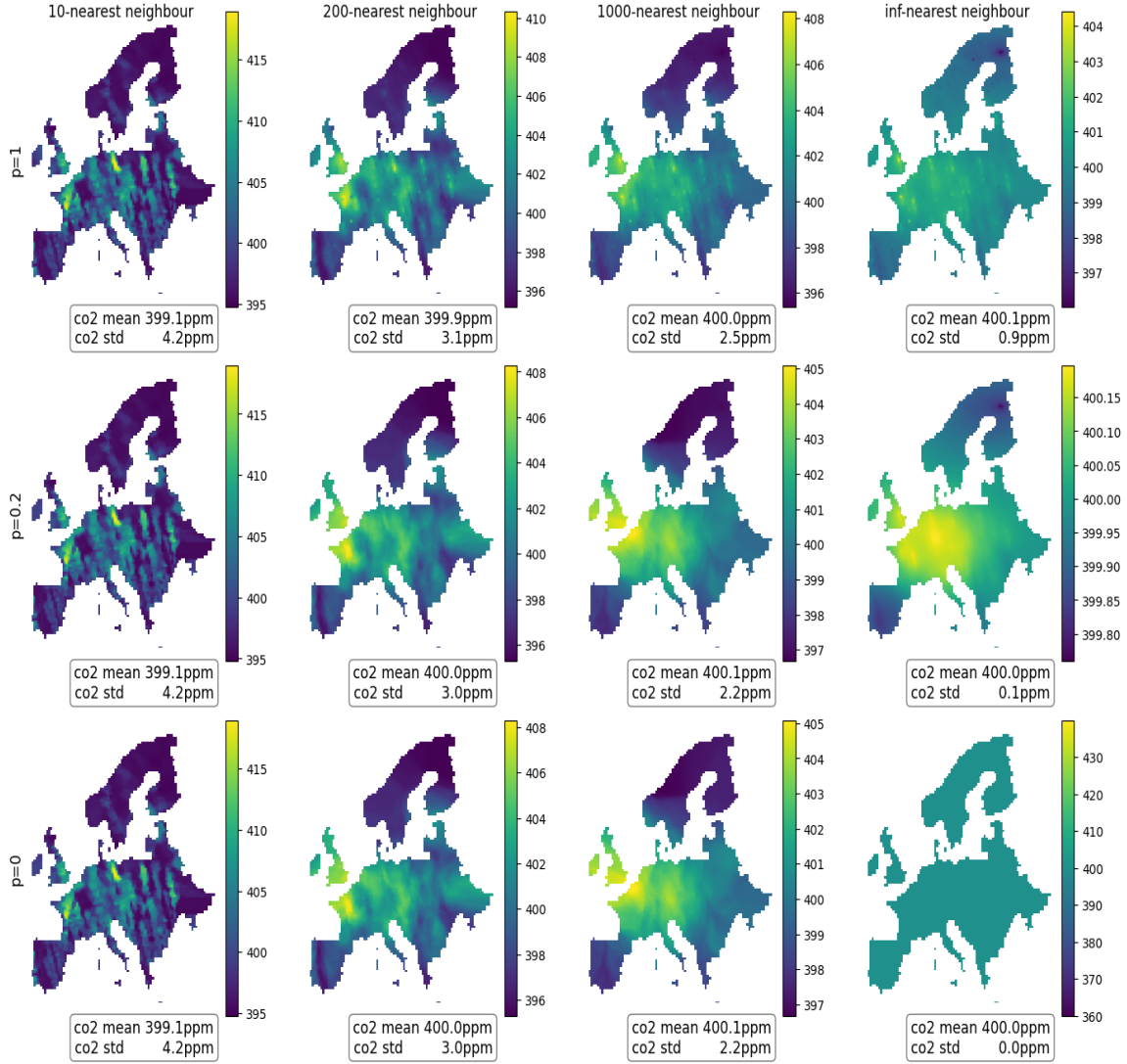


Figure 4: Interpolated predictions for Europe's 2015 ground level CO₂ concentrations using different parameterizations of the weighted K-nearest neighbor interpolation. The ablation study shows results as the nearest neighbor parameter K ranges from 10, 200, 1000, to ∞ (left to right), while the decay rate p is varied through 1, 0.2, and 0 (top to bottom). See Algorithm 1 for details.

$p = 0.05$ resulted in visually reasonable results on the European scale, while $K = 100$ and $p = 0.05$ resulted in more salient values for small scale municipal estimations. As stated before, the lack of ground truth data means that these parameter setting are unverified. They are only used for the example regional visualizations expressed in this section.

As a first example, Figure 5 displays the average predicted ground level CO₂ levels over Lund Municipality. The highest level of ground level CO₂ are predicted to be around northern Lund, and the lowest around Håckeberga nature preserve. We do not have ground truth data here to compare to, but at a glance this is a reasonable result as the preserve is reasonably a carbon sink. The higher levels to the north of Lund could possibly be due to the highway or perhaps the Örtofta sugar mill. Although it is important to stress that these results cannot be verified.

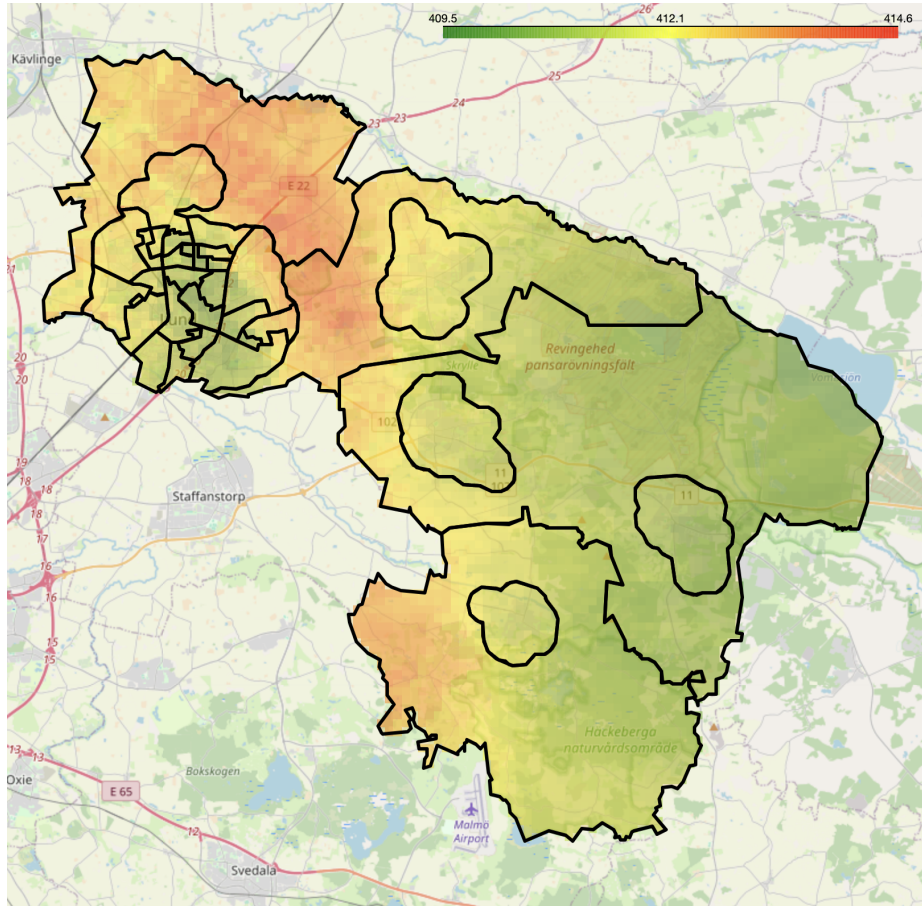


Figure 5: Predictions on the municipality of Lund, in southern Sweden, using the neural network regression model presented in Section 3.2. The KNN interpolation is made using $K = 100$ and $p = 0.05$. The estimated CO₂ levels are highest close to the city of Lund (top left) and further south near the airport (center bottom) at the city of Malmö while they are lowest around the Håckeberga natural park reserve (middle right).

The proposed approach has significant potential for scaling to larger regions, enabling the generation of high-resolution predictions across both time and space. Figure 6 illustrates yearly ground level CO₂ estimations across Europe, capturing the expected upward trend in CO₂ concentrations over time. Notably, these predictions are produced at a high spatial resolution, even for locations where no ground stations currently measure CO₂. Although the limited availability of ground level CO₂ data at such high spatial resolutions restricts our ability to independently validate these results, the figures highlight the model’s versatility. The model is capable of providing detailed predictions across varying spatial and temporal scales, surpassing the resolution of existing ground level measurements.

4.3 Feature Importance

To analyze the importance of the OCO and weather features used in predictions, a SHAP analysis Lundberg and Lee (2017) was employed. This method measures the change in output from the model when an input feature is changed. The feature importance is the amplitude of the prediction change when tweaking the corresponding feature.

The results, shown in Figure 7, highlight the relative importance of various features in our predictive model. The most significant feature identified was the xCO₂ from OCO2. This finding is expected, as xCO₂ provides a direct measurement of carbon concentration, making it a crucial indicator for our analysis.

In addition to xCO₂, temperature variables, specifically surface temperature and temperature at 2 meters, were also identified as important features. This result could be attributed to the fact that temperature serves as a proxy for the vertical movement of CO₂, influencing its distribution and concentration in the atmosphere, see Liang et al. (2017); Geldhauser and Romito (2019) for an overview. Moreover, the analysis revealed that geographic location (latitude and longitude) and temporal variables (time) are significant predictors. These features likely capture the global variations in atmospheric patterns that are not fully explained by other weather-related variables. Including location and time in the model helps account for the spatial and temporal heterogeneity in atmospheric CO₂ levels.

Overall, the SHAP analysis underscores the necessity of incorporating a diverse set of features, including direct measurements, proxy indicators, and spatial-temporal variables, to enhance the predictive accuracy of atmospheric CO₂ models.

5 Discussion

The results indicate that we can achieve accurate predictions of ground level CO₂ with an RMSE of under 4ppm and an adjusted R² value of over 80%. This can roughly be interpreted as the model typically guessing within 4ppm of the true value and that the model can explain over 80% of the variation in ground level CO₂.

Since the predictive features only consists of satellite data, the model can be applied to locations outside of ICOS stations and is therefore able to render high resolution predictions for any region. However, it is important to note that since ground truth data does not exist outside of ICOS stations, the extrapolated results cannot be verified at this moment.

The primary limitation of the current iteration of the model is the lack of good ground truth data. Since ground truth data is sparse and only localized around ICOS stations, the

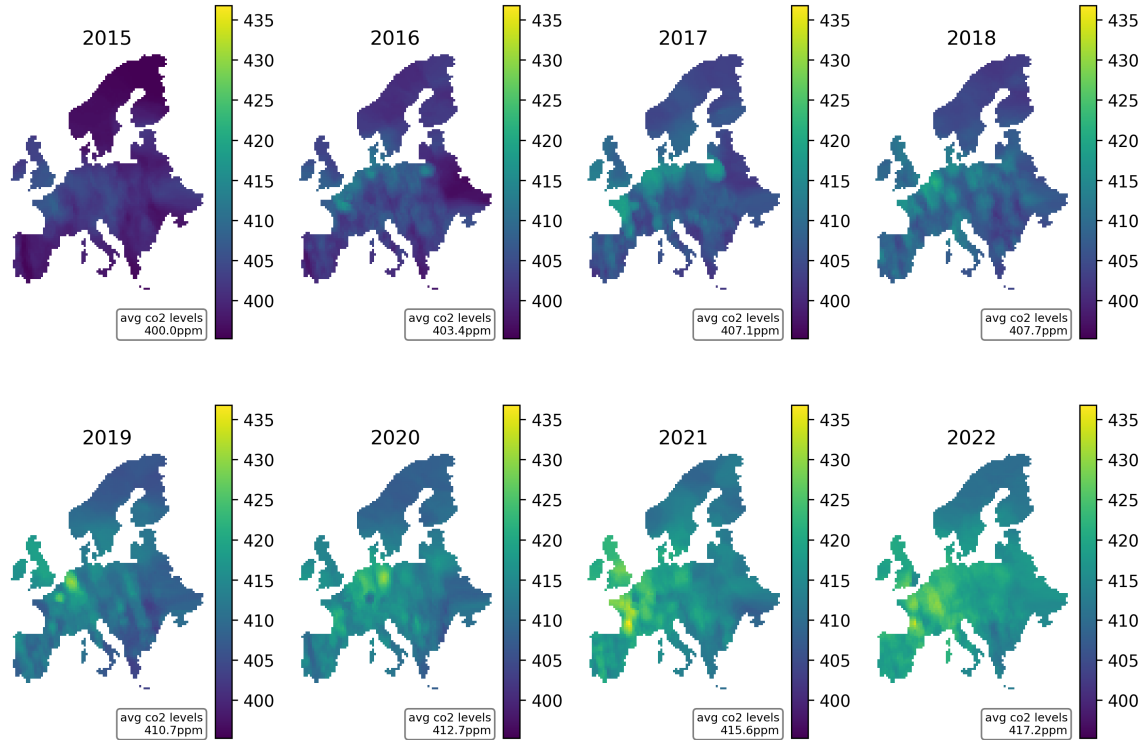


Figure 6: Annual ground level CO_2 estimations across Europe from 2015 to 2022, derived using the neural network regression model described in Section 3.2. The figure highlights spatial variations and temporal trends in CO_2 concentrations over the entire region, showcasing the model’s capability to capture and predict CO_2 levels at a high spatial resolution. The KNN interpolation was made using $K = 200$ and $p = 0.05$.

model will likely contain some biases towards these locations. Due to their size, stations are predominantly placed in rural areas or uninhabited regions, this means that there is very little ground truth data in cities or highly industrialized regions. In addition to this rural bias, we also have a continental bias as the ICOS stations are only located in Europe. The vast variety of landscapes, weather, and emission patterns that exist in the world cannot be said to be captured in the localized ground truth data available. Therefore, while the global reach of satellites allow for world-wide use of the model, it is highly discouraged at this stage. The primary application, for now, remains inside Europe.

That being said, the model can easily be adapted with additional ground truth data from any location in the world, thus opening up the possibility for global use in future iterations.

The second limitation is that while OCO has global reach, it doesn’t produce evenly distributed measurements either in space or time. Some regions, such as the south of Europe, receive much more observations compared to northern Europe due to their geographical

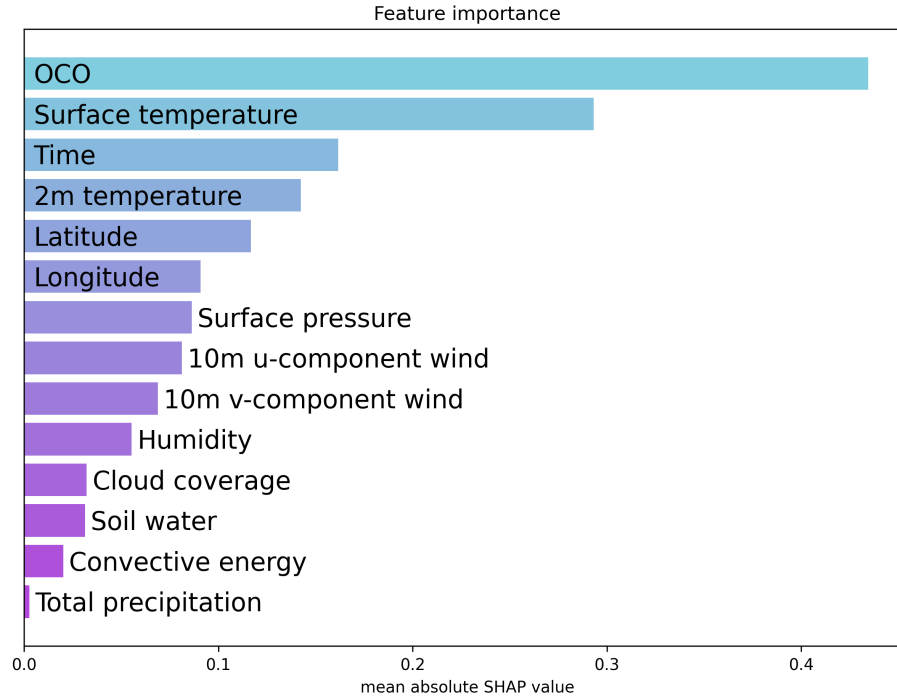


Figure 7: The importance of features in the input data using SHAP analysis based on the model results presented in Figure 2. The three most important features were the xCO₂ OCO measurements, surface temperature and time. The colors in the figure are used solely for differentiation and do not convey any additional information.

location. Closer to the poles, the observations are sparser and only receive a few orbits per year. This means that weekly or monthly averages will be highly inaccurate for many locations. Therefore, analyses should ideally keep to yearly averages or larger time spans.

With this in mind, the current stage of the model is primarily suited for estimations in Europe of yearly averages in large scale regions, or multi-year averages in smaller areas. The high level resolution of the prediction could give additional insights into where emissions stem from and where the most important carbon sinks are located. To increase usability, future research should focus mainly on expanding the availability of good ground truth data. While the ICOS stations provide invaluable information with great resolution in time, they provide only part of the picture due to their limited reach. A dataset consisting of ground level CO₂ measurements with low time resolution but high spatial spread would be a great contribution to this field as a complement to ICOS. Incorporation of global ground level CO₂ measurements would also contribute greatly by ensuring global reach and availability of predictions.

This methodology of using remote sensing with verified ground truth data will be crucial for equitable and informed climate action due to the fact that manual emission testing or CO₂ measuring stations are not an option for everyone. If this is done with steps ensuring

that the predictions are unbiased and representative of most locations and conditions, we believe that this can be a vital tool for local effort to mitigate climate change.

Towards better climate action

The foundation of our research lies in addressing the significant gap in localized CO₂ measurements, which hampers the effective design, implementation, and monitoring of precise local climate initiatives. The remote sensing approach we present has demonstrated its capacity to predict local CO₂ levels, offering a promising alternative to this critical shortcoming. At the same time, we outline a clear pathway for further refinement of this approach, emphasizing the need to ensure that verified ground truth data is unbiased and representative of diverse global locations and conditions.

Given the currently available data, the model introduced in this article holds significant potential to enhance climate action efforts by enabling:

- **Identification of High CO₂ Concentration Areas:** This allows for the strategic targeting of climate actions where they are most needed, optimizing resource allocation.
- **Monitoring of Temporal Changes in CO₂ Levels:** This facilitates the assessment of climate action effectiveness over time, providing feedback that can guide future interventions.
- **Effective Public Communication:** By using visual tools such as maps and graphs, we can communicate CO₂ level changes clearly to the public, fostering greater engagement and commitment to climate initiatives.
- **Validation of Reported Emission Data:** This contributes to the enforcement of environmental policies by verifying the accuracy of reported emissions, enhancing transparency and accountability.
- **Support for Multi-Level Governance:** Local administrations and European policymakers can rely on the same data sources, promoting coordinated and cohesive climate strategies across different governance levels.
- **Integration with Socio-Economic Data:** Combining local CO₂ data with socio-economic indicators enables the analysis of synergies and trade-offs within socio-ecological systems, supporting more holistic decision-making.

Due to the limitations of verified ground truth available, the current model is particularly well-suited for use across Europe, providing valuable insights for large-scale regions (such as countries) based on yearly averages, as well as for smaller-scale regions (such as municipalities) when considering multi-year averages.

6 Conclusions

Atmospheric CO₂ monitoring has seen substantial improvements in recent years, driven by advancements in technology. However, significant challenges persist. The commonly used bottom-up approaches, which rely heavily on reported data, often suffer from biases

and gaps in data coverage. Moreover, the long atmospheric lifespan of CO₂ compared to other pollutants like methane and aerosols leads to extensive spatial distribution due to atmospheric transport. To address these challenges, the integration of detailed weather data with sophisticated atmospheric models is crucial. As satellite technology continues to evolve, it offers increasing potential for more precise and localized monitoring of CO₂ emissions, which is critical for effective climate action and informed policy-making.

Our study aims to provide a more granular view of CO₂ emissions to support policy-makers in developing precise local climate action strategies. The proposed methodology goes beyond traditional approaches that rely on national data downsampling, by leveraging multimodal data collection for more accurate results.

While the proposed methodology shows significant promise, it does have some limitations. A potential limitation of the proposed methodology is the sparse availability of ground truth CO₂ measurements, particularly in urban and industrial regions. The reliance on data from ICOS stations, which are primarily located in rural and European settings, may introduce biases, potentially underrepresenting CO₂ variability in areas with higher emissions. Additionally, the OCO-2 and OCO-3 satellites do not provide uniform temporal and spatial coverage across all regions, particularly in areas with complex terrain or those distant from the equator. This uneven coverage could result in data gaps and impact the accuracy of CO₂ estimations over time and space, particularly in regions with limited direct observations.

The integration of satellite data with ground measurements is shown to be crucial for understanding and mitigating CO₂ emissions at a local level. This approach not only enhances precision in emissions monitoring but also lays a solid foundation for policy development, community engagement, and collaborative efforts towards global climate goals. Continued advancements in satellite technology, such as the upcoming Copernicus CO₂ Monitoring Mission (CO2M), promise to enhance the spatial and temporal resolution of CO₂ data, enabling more accurate and frequent monitoring of localized emissions Reuter et al. (2019). Future research should prioritize improving the accuracy of satellite-based CO₂ measurements, expanding the availability of ground level CO₂ data and integrating comprehensive meteorological datasets. These advancements will be key to deepening our understanding and management of CO₂ emissions on both regional and global scales.

Acknowledgments

This work is partially supported by FORMAS no. 2022-151862. The work of O. Å. and A. S. is also partially supported by grants from eSSSENCE no. 138227 and Rymdstyrelsen no. 2022-00282. The computations were enabled by resources provided by the National Academic Infrastructure for Supercomputing in Sweden (NAISS), partially funded by the Swedish Research Council through grant agreement no. 2022-06725.

References

- Oco-2 data center, 2023. URL <https://ocov2.jpl.nasa.gov>. Accessed: 2023-12-30.
- S. Beirle, K. Folkert Boersma, Ulrich Platt, Mark G. Lawrence, and Thomas Wagner. Megacity emissions and lifetimes of nitrogen oxides probed from space. *Science*, 333

- (6050):1737–1739, 2011. doi: 10.1126/science.1207824. URL <https://www.science.org/doi/abs/10.1126/science.1207824>.
- H. Bovensmann, M. Buchwitz, J. P. Burrows, M. Reuter, T. Krings, K. Gerilowski, O. Schneising, J. Heymann, A. Tretner, and J. Erzing. A remote sensing technique for global monitoring of power plant CO_2 emissions from space and related applications. *Atmospheric Measurement Techniques*, 3(4):781–811, 2010. doi: 10.5194/amt-3-781-2010. URL <https://amt.copernicus.org/articles/3/781/2010/>.
- Jianchao Cai, Kai Xu, Yanhui Zhu, Fang Hu, and Liuhuan Li. Prediction and analysis of net ecosystem carbon exchange based on gradient boosting regression and random forest. *Applied energy*, 262:114566, 2020.
- M. Claeysman, J.-L. Attié, V.-H. Peuch, L. El Amraoui, W. A. Lahoz, B. Josse, P. Ricaud, T. von Clarmann, M. Höpfner, J. Orphal, J.-M. Flaud, D. P. Edwards, K. Chance, X. Liu, F. Pasternak, and R. Cantié. A geostationary thermal infrared sensor to monitor the lowermost troposphere: O_3 and CO retrieval studies. *Atmospheric Measurement Techniques*, 4(2):297–317, 2011. doi: 10.5194/amt-4-297-2011. URL <https://amt.copernicus.org/articles/4/297/2011/>.
- A. Eldering, P.O. Wennberg, D. Crisp, D.S. Schimel, M.R. Gunson, A. Chatterjee, J. Liu, F.M. Schwandner, Y. Sun, C.W. O’dell, et al. The orbiting carbon observatory-2 early science investigations of regional carbon dioxide fluxes. *Science*, 358(6360):eaam5745, 2017.
- A. F. Feldman, Z. Zhang, Y. Yoshida, A. Chatterjee, and B. Poulter. Using orbiting carbon observatory-2 (oco-2) column CO_2 retrievals to rapidly detect and estimate biospheric surface carbon flux anomalies. *Atmospheric Chemistry and Physics*, 23(2):1545–1563, 2023. doi: 10.5194/acp-23-1545-2023. URL <https://acp.copernicus.org/articles/23/1545/2023/>.
- V. E. Fioletov, C. A. McLinden, N. Krotkov, and C. Li. Lifetimes and emissions of SO_2 from point sources estimated from omi. *Geophysical Research Letters*, 42(6):1969–1976, 2015.
- Carina Geldhauser and Marco Romito. The point vortex model for the Euler equation. *AIMS Math.*, 4(3):534–575, 2019. ISSN 2473-6988. doi: 10.3934/math.2019.3.534. URL <https://doi.org/10.3934/math.2019.3.534>.
- J. Hakkarainen, I. Ialongo, M. E. Szelag, and T. Oda. Characterizing major anthropogenic point sources in the south african highveld region using oco-3 carbon dioxide snapshot area maps and sentinel-5p/tropomi nitrogen dioxide columns. *IOP Science*, 2023. URL <https://iopscience.iop.org/article/10.1088/1748-9326/ac9f58>.
- Z. He, L. Lei, L. R. Welp, Z.-C. Zeng, N. Bie, S. Yang, and L. Liu. Detection of spatiotemporal extreme changes in atmospheric CO_2 concentration based on satellite observations. *Remote Sensing*, 10(6):839, 2018.
- Rajesh Janardanan, Shamil Maksyutov, Tomohiro Oda, Makoto Saito, Johannes W Kaiser, Alexander Ganshin, Andreas Stohl, Tsuneo Matsunaga, Yukio Yoshida, and Tatsuya

- Yokota. Comparing gosat observations of localized co₂ enhancements by large emitters with inventory-based estimates. *Geophysical Research Letters*, 43(7):3486–3493, 2016. doi: 10.1002/2016GL067843.
- G. Keppel-Aleks, P. O. Wennberg, C. W. O’Dell, and D. Wunch. Towards constraints on fossil fuel emissions from total column carbon dioxide. *Atmospheric Chemistry & Physics*, 13(8):4349–4357, April 2013. doi: 10.5194/acp-13-4349-201310.5194/acpd-12-29887-2012.
- Eric A Kort, Christian Frankenberg, Keeley R Costigan, Rodica Lindenmaier, Manvendra K Dubey, and Debra Wunch. Four corners: The largest us methane anomaly viewed from space. *Geophysical Research Letters*, 39(18), 2012. doi: 10.1029/2012GL052303.
- Xinfeng Liang, Michael Spall, and Carl Wunsch. Global ocean vertical velocity from a dynamically consistent ocean state estimate. *Journal of Geophysical Research: Oceans*, 122(10):8208–8224, 2017. doi: <https://doi.org/10.1002/2017JC012985>. URL <https://agupubs.onlinelibrary.wiley.com/doi/abs/10.1002/2017JC012985>.
- Scott M Lundberg and Su-In Lee. A unified approach to interpreting model predictions. *Advances in neural information processing systems*, 30, 2017.
- C. W. O’Dell, A. Eldering, P. O. Wennberg, D. Crisp, M. R. Gunson, B. Fisher, C. Frankenberg, M. Kiel, H. Lindqvist, L. Mandrake, A. Merrelli, V. Natraj, R. R. Nelson, G. B. Osterman, V. H. Payne, T. E. Taylor, D. Wunch, B. J. Drouin, F. Oyafuso, A. Chang, J. McDuffie, M. Smyth, D. F. Baker, S. Basu, F. Chevallier, S. M. R. Crowell, L. Feng, P. I. Palmer, M. Dubey, O. E. García, D. W. T. Griffith, F. Hase, L. T. Iraci, R. Kivi, I. Morino, J. Notholt, H. Ohyama, C. Petri, C. M. Roehl, M. K. Sha, K. Strong, R. Sussmann, Y. Te, O. Uchino, and V. A. Velazco. Improved retrievals of carbon dioxide from orbiting carbon observatory-2 with the version 8 acos algorithm. *Atmospheric Measurement Techniques*, 11(12):6539–6576, 2018. doi: 10.5194/amt-11-6539-2018. URL <https://amt.copernicus.org/articles/11/6539/2018/>.
- P. Peylin, R. M. Law, K. R. Gurney, F. Chevallier, A. R. Jacobson, T. Maki, Y. Niwa, P. K. Patra, W. Peters, P. J. Rayner, C. Rödenbeck, I. T. van der Laan-Luijkx, and X. Zhang. Global atmospheric carbon budget: results from an ensemble of atmospheric co₂ inversions. *Biogeosciences*, 10(10):6699–6720, 2013. doi: 10.5194/bg-10-6699-2013. URL <https://bg.copernicus.org/articles/10/6699/2013/>.
- M. Reuter, M. Buchwitz, A. Hilboll, A. Richter, O. Schneising, M. Hilker, J. Heymann, H. Bovensmann, and JP Burrows. Decreasing emissions of nox relative to co₂ in east asia inferred from satellite observations. *Nature Geoscience*, 7(11):792–795, 2014. doi: 10.1038/ngeo2257.
- M. Reuter, M. Buchwitz, O. Schneising, S. Krautwurst, C. W. O’Dell, A. Richter, H. Bovensmann, and J. P. Burrows. Towards monitoring localized co₂ emissions from space: co-located regional co₂ and no₂ enhancements observed by the oco-2 and s5p satellites. *Atmospheric Chemistry and Physics*, 19(14):9371–9383, 2019. doi: 10.5194/acp-19-9371-2019. URL <https://acp.copernicus.org/articles/19/9371/2019/>.

- Oliver Schneising, John P Burrows, Russell R Dickerson, Michael Buchwitz, Maximilian Reuter, and Heinrich Bovensmann. Remote sensing of fugitive methane emissions from oil and gas production in north american tight geologic formations. *Earth's Future*, 2(10), 2014. doi: 10.1002/2014EF000265.
- T. E. Taylor et al. Evaluating the consistency between oco-2 and oco-3 xco2 estimates derived from the nasa acos version 10 retrieval algorithm. *Atmospheric Measurement Techniques*, 16:3173–3209, 2023. doi: 10.5194/amt-16-3173-2023.
- OCO-2 Science Team, Michael Gunson, and Annmarie Eldering. <https://doi.org/10.5067/E4E140XDMP02>, December 2020. URL https://disc.gsfc.nasa.gov/datasets/OC02_L2_Lite_FP_10r/summary. Greenbelt, MD, USA, Goddard Earth Sciences Data and Information Services Center (GES DISC).
- R. Wang, S. Tao, P. Ciais, H. Z. Shen, Y. Huang, H. Chen, G. F. Shen, W. Wang, B. Li, Y. Y. Zhang, Y. Lu, D. Zhu, Y. C. Chen, X. P. Liu, W. T. Wang, X. L. Wang, W. X. Liu, B. G. Li, and S. L. Piao. High-resolution mapping of combustion processes and implications for co2 emissions. *Atmos. Chem. Phys.*, 13:5189—5203, 2013. doi: 10.5194/acp-13-5189-2013.
- W. Wang, J. He, H. Feng, and Z. Jin. High-coverage reconstruction of xco2 using multisource satellite remote sensing data in beijing–tianjin–hebei region. *International Journal of Environmental Research and Public Health*, 19(17), 2022. ISSN 1660-4601. doi: 10.3390/ijerph191710853. URL <https://www.mdpi.com/1660-4601/19/17/10853>.
- Hung-Ta Wen, Jau-Huai Lu, and Deng-Siang Jhang. Features importance analysis of diesel vehicles’ nox and co2 emission predictions in real road driving based on gradient boosting regression model. *International Journal of Environmental Research and Public Health*, 18(24):13044, 2021.
- Xinxin Ye et al. Constraining fossil fuel co2 emissions from urban area using oco-2 observations of total column co2. *Journal of Geophysical Research: Atmospheres*, 125, 2020. doi: 10.1029/2019JD030528.
- T Yokota, Y Yoshida, N Eguchi, Y Ota, T Tanaka, H Watanabe, and S Maksyutov. Global concentrations of co2 and ch4 retrieved from gosat: First preliminary results. *SOLA*, 5: 160–163, 2009. doi: 10.2151/sola.2009-041.

Appendix: Model Hyperparameters

This paper considers three models in addition to the baseline prediction. The baseline model only uses the xCO₂ measurements from OCO as a naive prediction for the ICOS and therefore it has no hyperparameters.

The Category Boosting model is based on the CatBoostClassifier model from the catboost package for python, using the following hyperparameters:

- *nbr_classes* = 25
- *max_depth* = 6
- *learning_rate* = 0.1
- *iterations* = 100
- *l2_leaf_reg* = 3

The Extreme Gradient Boosting model is based on the XGBRegressor model from the XGBoost package for python, using the following hyperparameters:

- *max_depth* = 6
- *learning_rate* = 0.1
- *n_estimators* = 100
- *gamma* = 0

The Neural Network Regression model consists of 4 densely connected layers of sizes 64, 128, 64 and 32 respectively. In addition, the model uses an output layer consisting of a single node with linear activation. The model uses a learning rate of 0.001.

In the internal layers of this neural network we employ a ReLU activation function which is one of the most widely used activation functions in neural networks, particularly in deep learning. It is defined as follows:

$$\text{ReLU}(x) = \max(0, x) = \begin{cases} x & \text{if } x \geq 0 \\ 0 & \text{if } x < 0 \end{cases}$$

Properties of ReLU:

- Non-linearity: ReLU introduces non-linearity to the model, which is crucial for learning complex patterns.
- Computationally efficient: It is simple to compute, which speeds up the training process.
- Sparse activation: Since the ReLU outputs zero for all negative inputs, it often leads to sparse activations, making the network more efficient.

We also employ L_2 regularization which is a technique used to prevent overfitting in neural networks by penalizing large weights in the model. The basic idea is to add a penalty term to the loss function, which discourages the model from learning excessively large weights.

Given a loss function $\mathcal{L}(\mathbf{y}, \hat{\mathbf{y}})$, where \mathbf{y} are the true labels and $\hat{\mathbf{y}}$ are the predicted labels, the L_2 regularized loss function is:

$$\mathcal{L}_{\text{reg}}(\mathbf{y}, \hat{\mathbf{y}}) = \mathcal{L}(\mathbf{y}, \hat{\mathbf{y}}) + \lambda \sum_i w_i^2$$

Here:

- \mathcal{L}_{reg} is the regularized loss function.
- \mathcal{L} is the original loss function (which in our case refers to mean squared error).
- w_i represents the weights of the model.
- λ is the regularization parameter (often called the regularization strength), which controls the amount of regularization applied.

The L_2 regularization term $\lambda \sum_i w_i^2$ is the sum of the squares of the weights, multiplied by the regularization parameter λ . This term encourages the model to keep the weights small, which helps to reduce overfitting.